ISSN 1063-7761, Journal of Experimental and Theoretical Physics, 2015, Vol. 120, No. 5, pp. 894–904. © Pleiades Publishing, Inc., 2015.
Original Russian Text © G.E. Norman, I.M. Saitov, V.V. Stegailov, 2015, published in Zhurnal Eksperimental'noi i Teoreticheskoi Fiziki, 2015, Vol. 147, No. 5, pp. 1032–1044.

STATISTICAL, NONLINEAR, AND SOFT MATTER PHYSICS

First-Principles Calculation of the Reflectance of Shock-Compressed Xenon

G. E. Norman[a,b], I. M. Saitov[a]*, and V. V. Stegailov[a,b,c]

[a] *Institute of High Temperatures, Russian Academy of Sciences, ul. Izhorskaya 13/19, Moscow, 125412 Russia*
[b] *Moscow Institute of Physics and Technology, Institutskii per. 9, Dolgoprudnyi, Moscow oblast, 141700 Russia*
[c] *National Research University Higher School of Economics, Moscow, 101000 Russia*
**e-mail: saitovilnur@gmail.com*

Received May 26, 2014; in final form, November 11, 2014

Abstract—Within electron density functional theory (DFT), the reflectance of radiation from shock-compressed xenon plasma is calculated. The dependence of the reflectance on the frequency of the incident radiation and on the plasma density is considered. The Fresnel formula is used. The expression for the longitudinal dielectric tensor in the long-wavelength limit is used to calculate the imaginary part of the dielectric function (DF). The real part of the DF is determined by the Kramers–Kronig transformation. The results are compared with experimental data. An approach is proposed to estimate the plasma frequency in shock-compressed xenon.

DOI: 10.1134/S1063776115040135

1. INTRODUCTION

The measurements of the reflectance and theoretical analysis of the measurement results are widely used methods for investigating the phase diagrams of various substances [1–9]. In this study, we consider shock-compressed xenon plasma. The reflectance from shock-compressed xenon was obtained for wavelengths $\lambda = 1064$, 694, and 532 nm in unique experiments [10–13] in which plasma was generated by dynamic compression of xenon gas by a high-power shock wave. To this end, the authors used a method of high-speed collision of a metal striker accelerated to velocity of 6 km/s with a gas cuvette followed by irreversible heating of the gas at the front of the shock wave. To create a plane configuration of a shock-wave front in the gas, the authors used a modified square-wave oscillator. The plasma density is varied by varying the initial gas pressure. The initial parameters of xenon gas are as follows: pressure $P_0 = 1.0$–5.7 MPa, density $\rho_0 = 0.06$–0.80 g/cm^3, and temperature $T = 270$ K. The parameters of the plasma created by shock compression are as follows: pressure $P = 1.6$–17 GPa, density $\rho_0 = 0.5$–4.0 g/cm^3, and temperature $T = 30000$ K. The reflectance is determined from the signals of photocells that detect the reflected radiation and a signal from a photocell that detects a probing pulse. A satisfactory theoretical explanation of the results obtained has not been found as yet.

Figure 1 demonstrates the reflectance as a function of charge density in xenon plasma: the case of collisionless plasma with cutoff at the plasma frequency, the experimental data of [10] (the values of n_e correspond to the estimates obtained in [10]), and the approximation of the measurement results by the Drude formula [14].

The main goal of the experiment in [10] was to evaluate the density of free charge carriers and the plasma frequency for shock-compressed xenon on the basis of the measurement of the reflectance as a func-

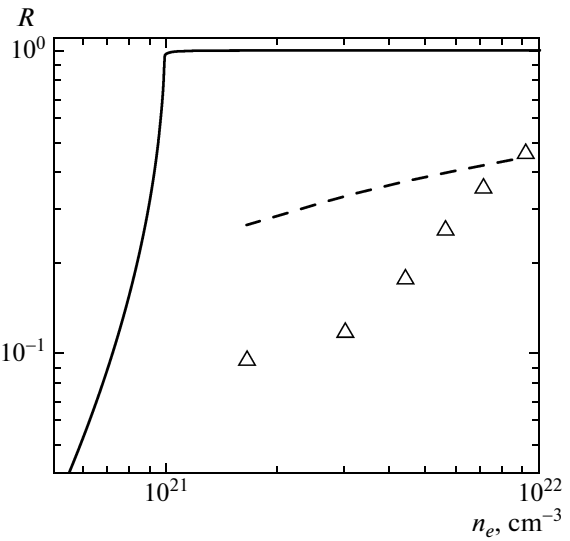

Fig. 1. Reflectance as a function of electron density n_e. Solid curve corresponds to the case of collisionless plasma with cutoff at the plasma frequency. Triangles denote the results of experiment from [10]. The dashed curve corresponds to the approximation of the experimental results with the use of the Drude model with the collision frequency in the Born approximation [14]. The wavelength is 1064 nm.

tion of density. It was assumed that the profile of the reflectance vs. density is similar to that in the case of collisionless plasma (solid line in Fig. 1). Then the dependence of the dielectric function (DF) on frequency would have the form $\varepsilon(\omega) = 1 - \omega_p^2/\omega^2$. In this case, if $\omega_p > \omega$, then total internal reflection occurs, and $R = 1$.

However, the measured dependence of the reflectance on density (the triangles in Fig. 1) has no cutoff at the plasma frequency and slowly increases with density. An attempt to take into account the collision frequency in the Born approximation within the Drude model [14] (the dashed line in Fig. 1) did not give a satisfactory description of the experimental results either.

Further attempts to explain the results of measurements within the Drude model were based on the assumption of the broadening of the wave front [14–16]. In spite of the improved agreement with experiment, this approach did not allow one to establish a one-to-one correspondence between reflectance and the free charge density. At present, the suggested widths of the wave front also lack independent experimental confirmation.

Shock-compressed xenon plasma represents an example of warm dense matter, the theoretical description of which requires irregular methods (see, for example, [17–21]). One of effective methods for the first-principles study of the properties of warm dense matter is the electron density functional theory (DFT) method [22–24]. The fundamental character of this method allows its application to the study of a wide range of phenomena (see, for example, [25–28]) and, in particular, to the calculation of the DF of various substances [4, 6, 8, 9, 29–34].

In [29], to calculate the reflectance from xenon plasma, Desjarlais applied a quantum method of molecular dynamics within DFT for finite temperatures, which is based on the formulation of DFT given in [35]. To calculate the components of the DF, the author used an expression for the transverse component of the DF—the Kubo–Greenwood formula [36, 37]—and the Kramers–Kronig transformation. The results obtained in [29] are in better agreement with experiment [10] compared with the data calculated within the Drude model. Nevertheless, the reflectance obtained in [29] is appreciably greater than the measurement data of [10] at low densities. The introduction of corrections that increase the energy gap width between bound and free states improves the agreement between the results of [29] and [10] at low densities but leads to underestimated values of the reflectance at high densities.

The approach used in this paper is largely similar to that applied in [29]; however, our approach suggests using the longitudinal expression for the imaginary part of the DF, which is more accurate within DFT. In Section 2, we present the basic formulas for calculating the DF and the reflectance. For the imaginary part of the DF, we compare expressions for different components of the dielectric tensor. In Section 3, we consider a method for calculating the reflectance within DFT on the basis of the formulas given in Section 2. As a test calculation, we present the reflectance as a function of density calculated with the use of the Kubo–Greenwood formula for the imaginary part of the DF and compared with the results of [29]. Section 4 discusses the applicability of the term "free electrons" in the case of a dense plasma. We propose a method for calculating the plasma frequency within the DFT approach and present the results of calculation of this parameter as a function of density. We also calculate the effective concentrations of free electrons for different plasma densities. In Section 5, we present the main results: the reflectance as a function of density for different wavelengths of the incident radiation, calculated with the use of the expression for the longitudinal component of the DF. We also present an analysis of the convergence and an accuracy estimate for the results obtained. Section 6 is devoted to the discussion of the results. We compare the results of calculation obtained in the present paper with the results of [29].

2. BASIC RELATIONS

The calculations of the DF and the reflectance of a laser radiation from shock-compressed xenon are carried out within DFT. Among 54 electrons of a xenon atom, 46 electrons situated on the inner shells are considered by the pseudopotential of projected augmented waves [38]. For 8 electrons on the outer shell (with a principal quantum number of 5), a system of Kohn–Sham equations is solved with a pseudopotential that effectively takes into account the field of the remaining 46 electrons.

Pseudopotentials may be either local or nonlocal. Local potentials are diagonal, and their matrix elements can be represented as

$$\langle \mathbf{r}|V|\mathbf{r}'\rangle = V(\mathbf{r})\delta(\mathbf{r}-\mathbf{r}'). \quad (1)$$

Nonlocal potentials $V(\mathbf{r}, \mathbf{r}')$ are not diagonal; therefore, the effect of these potentials on the wave functions cannot be considered as a product, and one should calculate the integral,

$$\langle \mathbf{r}|V|\psi\rangle = \int V(\mathbf{r}, \mathbf{r}')\psi(\mathbf{r}')d^3\mathbf{r}'. \quad (2)$$

Due to this property, in particular, the operator of potential $V(\mathbf{r}, \mathbf{r}')$ does not commute with the operator of coordinate $\mathbf{r}$. Thus, this approximation imposes some constraints on the formula for the DF, which is discussed below.

The DF is a complex quantity and can be represented as $\varepsilon = \varepsilon^{(1)} + i\varepsilon^{(2)}$. There exist two expressions for the dielectric tensor depending on the character of the external field: longitudinal and transverse.

In this study, we consider the reflection of laser radiation from plasma. When an electromagnetic

(transverse) radiation acts on a substance, the response function is the transverse DF; the imaginary part of this function versus frequency ω for given temperature and ion configuration $\{\mathbf{R}_i\}$ is given by the following expression in the long-wavelength limit [39]:

$$\varepsilon_T^{(2)}(\omega, \mathbf{R}_i) = \frac{1}{3}\frac{4\pi^2 e^2}{\omega^2 \Omega}\lim_{|\mathbf{q}|\to 0}\sum_{n, n', \alpha, \mathbf{k}} 2w_{\mathbf{k}} \times [f(E_{n', \mathbf{k}+\mathbf{q}}) - f(E_{n, \mathbf{k}})] \times \left|\langle \psi_{n'\mathbf{k}}|\hat{\mathbf{v}}_\alpha|\psi_{n\mathbf{k}}\rangle\right|^2 \delta(E_{n', \mathbf{k}+\mathbf{q}} - E_{n\mathbf{k}} - \hbar\omega), \quad (3)$$

where e is elementary charge, Ω is the volume of the systems, and $\mathbf{q}$ is the wave vector of the incident radiation. The summation is over all states n and n'. This expression takes into account the contributions of terms with both $n = n'$ (intraband transitions) and $n \neq n'$ (interband transitions). The summation is over all $\mathbf{k}$ points in the Brillouin zone with regard to the weight $w_{\mathbf{k}}$ of a $\mathbf{k}$ point. The factor of 2 in front of $w_{\mathbf{k}}$ takes into account the spin degeneracy. The result of summation over the index α, multiplied by 1/3, is the result of averaging over three spatial coordinates. Thus, the assumption of isotropy of the system is taken into account, which is justified in the case of plasma.

In formula (3), $\hat{\mathbf{v}}$ is the velocity operator, $E_{n, \mathbf{k}}$ are the eigenvalues (energy levels) corresponding to the given wave functions, $f(E_{n, \mathbf{k}})$ is the Fermi–Dirac distribution function, which determines the population of levels, and $\psi_{n, \mathbf{k}}$ is a solution to the Schrödinger (Kohn–Sham) equation. In this paper, we find a solution to the system of Kohn–Sham equations as a superposition of plane waves; therefore, the solution can be represented as Bloch functions, $\psi_{n, \mathbf{k}} = e^{i\mathbf{k}\cdot\mathbf{r}}u_{n, \mathbf{k}}$, where $u_{n, \mathbf{k}}$ is the periodic part of the wave function.

The velocity operator $\hat{\mathbf{v}}$ can be expressed in terms of the commutator,

$$\hat{\mathbf{v}} = \frac{d\mathbf{r}}{dt} = \frac{i}{\hbar}[H, \mathbf{r}], \quad (4)$$

where H is the Hamiltonian. If the potential is local, then, replacing $\hat{\mathbf{v}}$ by $\mathbf{p}/m$ (m is the electron mass and $\mathbf{p}$ is its momentum operator) in (3), we obtain the Kubo–Greenwood formula [36, 37]:

$$\varepsilon_T^{(2)}(\omega) = \frac{1}{3}\frac{4\pi^2 e^2\hbar^2}{m^2\omega^2\Omega}\lim_{|\mathbf{q}|\to 0}\sum_{n, n', \alpha, \mathbf{k}} 2w_{\mathbf{k}} \times [f(E_{n', \mathbf{k}+\mathbf{q}}) - f(E_{n, \mathbf{k}})]\left|\langle u_{n', \mathbf{k}}|\nabla_\alpha - i\mathbf{k}_\alpha|u_{n, \mathbf{k}}\rangle\right|^2 \times \delta(E_{n', \mathbf{k}+\mathbf{q}} - E_{n, \mathbf{k}} - \hbar\omega), \quad (5)$$

where m is the electron mass. However, if the potential is nonlocal, the operators of velocity and momentum are different and are related by [40]

$$\hat{\mathbf{v}} = \frac{\mathbf{p}}{m} + \frac{i}{\hbar}[V(\mathbf{r}, \mathbf{r}'), \mathbf{r}]. \quad (6)$$

Thus, in the case of a nonlocal potential, the Kubo–Greenwood formula turns out to be inapplicable to the calculation of the imaginary part of the DF.

In spite of the fact that the medium considered is isotropic, the responses of the system depend on the form of a perturbation (longitudinal or transverse) and do not coincide in the general case. The simplest illustration of this assertion is given by the conductivity tensor obtained in the approximation of the hydrodynamic model of plasma [41]. However, in the long-wavelength limit, the transverse and longitudinal components of the dielectric tensor coincide. Let us represent the velocity operator as [39]

$$\hat{\mathbf{v}} = \lim_{|\mathbf{q}|\to 0}[H, \exp(i\mathbf{q}\cdot\mathbf{r})]/\hbar|\mathbf{q}|. \quad (7)$$

Substituting formula (7) into (3), we obtain an expression for the imaginary part of the DF as a function of frequency ω for given values of temperature and ion configuration $\{\mathbf{R}_i\}$ for a longitudinal dielectric tensor:

$$\varepsilon_L^{(2)}(\omega, \mathbf{R}_i) = \frac{1}{3}\frac{4\pi^2 e^2}{\Omega}\lim_{|\mathbf{q}|\to 0}\frac{1}{|\mathbf{q}|^2}\sum_{n, n', \alpha, \mathbf{k}} 2w_{\mathbf{k}} \times [f(E_{n', \mathbf{k}+\mathbf{q}}) - f(E_{n, \mathbf{k}})]\left|\langle u_{n', \mathbf{k}+\mathbf{e}_\alpha q}u_{n, \mathbf{k}}\rangle\right|^2 \times \delta(E_{n', \mathbf{k}+\mathbf{q}} - E_{n, \mathbf{k}} - \hbar\omega), \quad (8)$$

where $\mathbf{e}_\alpha$ is a unit vector that defines the direction of a Cartesian axis of the coordinate α. Formula (8) was obtained in [42–44] in the first approximation of perturbation theory within the random phase approximation. Since, to obtain (8), we use a transformation of the velocity, rather than the momentum operator, formula (8) is free of the drawback of the Kubo–Greenwood formula and can be applied for any pseudopotentials. Notice that from (8) we can also obtain formula (5), using the relation

$$\lim_{|\mathbf{q}|\to 0}\frac{\langle u_{n\mathbf{k}}|u_{n'\mathbf{k}+\mathbf{q}}\rangle}{|\mathbf{q}|} = -\frac{\hbar^2}{m}\lim_{|\mathbf{q}|\to 0}\frac{\langle u_{n'\mathbf{k}}|(\nabla - i\mathbf{k})|u_{n\mathbf{k}}\rangle}{E_{n'\mathbf{k}+\mathbf{q}} - E_{n\mathbf{k}}}, \quad (9)$$

which is valid only in the case of a local pseudopotential.

The real part of the DF is determined by the Kramers–Kronig transformation:

$$\varepsilon^{(1)}(\omega) = 1 + \frac{2}{\pi}\int_0^\infty d\omega'\frac{\varepsilon^{(2)}(\omega')\omega'}{(\omega')^2 - (\omega - i\eta)^2}, \quad (10)$$

where the integral is defined in the sense of the principal value in the limit as $\eta \longrightarrow 0$. In the general case, the response function of the system to the external action is not the DF, but the inverse of this quantity. Due to the causality principle, the Kramers–Kronig relations are always valid for the inverse of the DF. In this case, formula (10) is valid only in the limit when the wavelength of the incident radiation is several times greater than the characteristic size of the system, which is the case in our case.

For the range of plasma parameters considered, the wavelength of laser radiation is much greater than both

Calculation parameters (density and temperature) and calculated values of the chemical potential E_F

$\lambda = 1064$ nm			$\lambda = 694$ nm, 532 nm		
ρ, g/cm^3	T, K	E_F, eV	ρ, g/cm^3	T, K	E_F, eV
0.51	30050	−8.26	0.53	32900	−8.84
0.97	29570	−6.5	1.1	33100	−6.8
1.46	30260	−5.37	1.6	33120	−5.5
1.98	29810	−4.2	2.2	32090	−4.08
2.7	29250	−1.75	2.8	32020	−2.96
3.84	28810	−0.92	3.4	31040	−1.84

the characteristic size of an atom and the mean free path of an electron in all three cases. However, in this case one should consider another characteristic size, which should be compared with the value of the wave vector $\mathbf{q}$. A transition to the long-wavelength limit implies, in particular, that $|\mathbf{q}| \ll |\mathbf{k}|$, where $\mathbf{k}$ can be considered as the inverse lattice vector for periodic systems. In our case, the system is disordered; therefore, one can take $|\mathbf{k}| \sim d$, where d is the macroscopic size of the system. Then the condition $|\mathbf{q}| \ll |\mathbf{k}|$ implies that $\lambda \gg d$. In this case, since the medium is an absorbing one, one can take as d the penetration depth of the field into the substance, because it is this depth at which most of the reflection occurs. Then the ratio of this parameter to the wavelength can be defined as $d/\lambda = n_1/4\pi n_2$, where n_2 and n_1 are the imaginary and real parts of the refractive index, respectively.

Note also that, in this case, the system responds to the external action whose source is outside the system. As the response function, one considers the DF (but not its inverse), which is applicable only when the wavelength is much greater than the characteristic size of the system.

The values of the DF are determined for a fixed ion configuration. To determine the value corresponding to the chosen temperature and density, the DF is averaged over a set of equilibrium configurations. The reflectance is calculated by the Fresnel formula for normal incidence:

$$R = \left|\frac{(\sqrt{\varepsilon} - \mathbf{1})}{(\sqrt{\varepsilon} + \mathbf{1})}\right|^2. \quad (11)$$

3. METHOD OF CALCULATION

For calculations, we use the VASP package [45–47]. As shown in the previous section, expression (5) for the transverse dielectric tensor gives a correct result only in the case when the pseudopotential is local. If the pseudopotential is nonlocal (which is the case for almost all pseudopotentials used in DFT codes), one should use expression (8) for the longitudinal dielectric tensor.

In the calculations, we use the approximation of generalized gradients for the exchange and correlation parts of the electron density functional. We use the Perdew–Burke–Ernzerhof (PBE) functional [48]. The wave functions, which are a solution to the set of Kohn–Sham equations, and the corresponding energy levels are needed to calculate the components of the DF. A solution to this system is sought in the form of a superposition of plane waves. The cutoff energy of the basis of plane waves is chosen to be equal to 180 eV.

The restriction of the volume of the system leads to a discrete spectrum of eigenvalues. As an approximation to the δ function in formulas (5) and (8), we used the Gauss function with a width of 0.03 eV. We also calculated the DF for values of δ from 0.01 to 0.1 and found that the result was not changed.

The calculations are performed for a canonical ensemble. The ion temperature is controlled by the Nose–Hoover thermostat [49, 50]. The equal electron temperature is defined by the Fermi–Dirac distribution for the occupancies of states $f(E)$. The temperature of the system is about 30000 K. The values of temperature and density corresponding to the experimental conditions of [10–13], for which the calculation is performed, as well as the values of the chemical potential (the Fermi energy) calculated within DFT for the given parameters, are shown in the table.

The values of the DF are averaged over a set of ion configurations. This set is determined by the quantum molecular dynamics method. The trajectories of particles are calculated by the integration of Newton's classical equations of motion with forces determined by the Hellmann–Feynman theorem. Depending on the density of particles in a computation cell, the trajectories consist of from 4000 to 10000 2-fs steps. On each trajectory, from 5 to 10 statistically independent configurations are distinguished.

We considered the range of plasma densities $\rho = 0.51–3.84$ g/cm^3. The number of particles in a computation cell was varied from 16 for the lowest density to 128 for the highest density. The computation time of the DF for a given particle configuration and the lowest density was about 15 hours on the 36 core cluster K-100. As the density increased for a given number of particles in a computation cell, the computation time decreased.

As mentioned in the Introduction, the reflectance from a shock-compressed xenon plasma was computed in [29], where the Kubo–Greenwood formula (5) was used to determine the imaginary part of the DF. We also carried out a calculation by the method proposed in [29]. Figure 2 shows that our results are in a rather good agreement with the data of [29] in spite of the fact that we used the latest version of the exchange–correlation PBE functional [51].

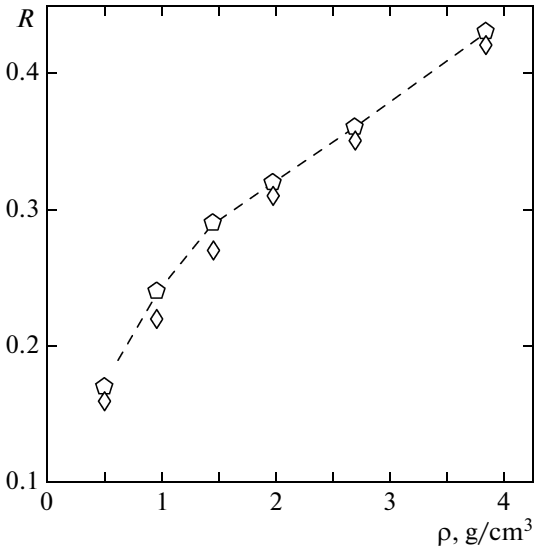

Fig. 2. Reflectance as a function of density for a wavelength of 1064 nm. The results of calculation within DFT with the Kubo–Greenwood formula for the imaginary part of the DF: pentagons connected by a dashed curve represent the results of [29], and diamonds represent the results of the present study.

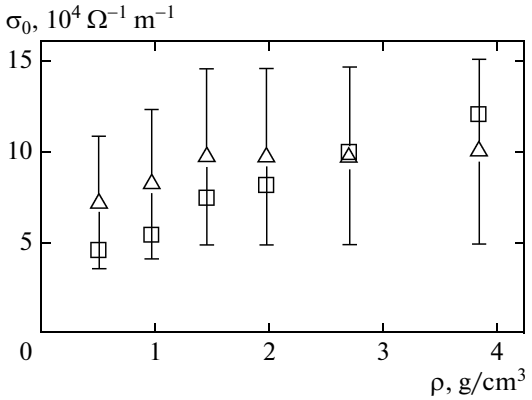

Fig. 3. Static conductivity as a function of density. Triangles represent the results of measurements from [14], and squares represent the results of calculation.

4. FREE ELECTRONS AND PLASMA FREQUENCY

Low-temperature atomic plasma consists of electrons, ions, and atoms that are in the ground and excited states. In the case of low-density plasma, electrons can be conventionally divided into bound electrons, which are characterized by discrete spectrum, and free electrons with continuous spectrum. An electron in an atom can be either in the ground state or on excited levels.

The excited levels are broadened due to the Stark effect, and the upper levels merge together, forming a quasi-continuous spectrum, whose beginning is determined by the Inglis–Teller formula. Moreover, a stronger transformation of pair-excited states occurs because the lifetime of these states decreases with increasing excitation due to Coulomb collisions. This lifetime vanishes even at energies below the ionization threshold by a certain value ΔE, which may be less than the Inglis–Teller limit. The electron states in the interval ΔE can be referred to quasi-continuous collective multiparticle states [52].

Both the Inglis–Teller limit and ΔE increase with the charge concentration. Therefore, the distinguishing of free states in the spectrum of electron states becomes more and more conditional and approximate, which complicates the calculation of the plasma frequency by the standard formula.

In this paper, we propose two methods for evaluating the plasma frequency on the basis of the calculated imaginary part of the DF as a function of frequency. The first method is based on the calculation of the dynamic conductivity, whose real part is related to the imaginary part of the DF by the formula $\sigma(\omega) = \varepsilon_0\omega\varepsilon^{(2)}(\omega)$, where ε_0 is the permittivity of vacuum. In the range of low frequencies, this formula for $\sigma(\omega)$ can be approximated by the Drude formula [53, 54]:

$$\sigma(\omega) = \frac{\varepsilon_0\omega_p^2\tau}{1+\omega^2\tau^2}. \quad (12)$$

The parameters of this approximation are the relaxation time τ and the required plasma frequency ω_p. Figure 3 demonstrates the comparison of the experimental [14] and calculated values of static conductivity as a function of density. One can see that the results of calculations are in a rather good agreement with the experimental results.

The second method is based on the rule of sums [55]:

$$\int_0^\infty \omega\varepsilon^{(2)}(\omega)d\omega = \frac{\pi}{2}\omega_p^2. \quad (13)$$

Taking into account the necessity to apply numerical methods to calculating the integral (13), consider the following function, which depends on the upper limit ω_{max}:

$$S(\omega_{max}) = \frac{2m\varepsilon_0\Omega}{\pi N_e e^2}\int_0^{\omega_{max}} \varepsilon^{(2)}(\omega)\omega d\omega. \quad (14)$$

Expression (14) is deduced from (13) by substituting ω_{max} for infinity in the upper limit of the integral (13) and taking into account the expression for the plasma frequency

$$\omega_p^2 = N_e e^2/m\varepsilon_0\Omega. \quad (15)$$

For xenon, the number of electrons within the DFT approach is $N_e = 8N$, where N is the number of heavy particles in a computation cell with volume Ω. Figure 4 shows the function $S(\omega_{max})$ for a xenon density of $\rho = 2.2$ g/cm^3. One can see that the function S

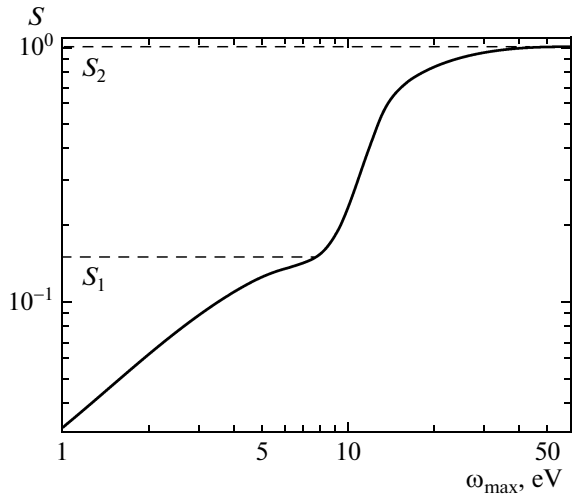

Fig. 4 Function S versus the upper limit ω_{max}.

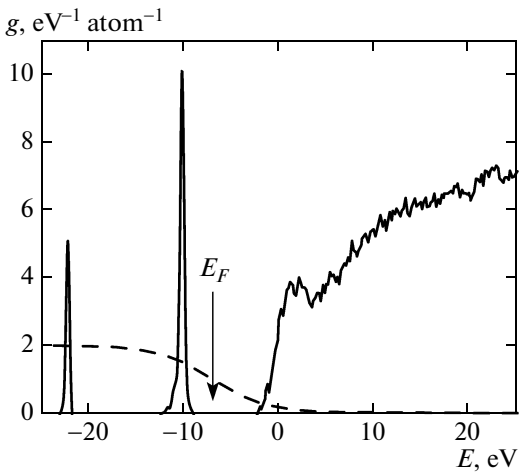

Fig. 5. Electron state density for a plasma density of $\rho = 1.1$ g/cm^3. The dashed curve is the population of levels $f(E)$. The arrow indicates the Fermi level.

has two stationary values: denote them as S_1 and S_2. The value $S_2 = 1$ corresponds to eight electrons, which indicates that the calculation is correct.

The expression for the imaginary part of the DF defined by formula (8) and appearing in (14) takes into account all possible transitions between electron levels within the DFT approach. These transitions can be divided into two classes: intraband and interband transitions. Interband transitions in plasma are possible between different discrete bound states (transitions between states with different principal quantum numbers) and between bound and free states (photoionization). Intraband transitions are possible both in the continuous spectrum and within a bound state (transitions between states with the same principal quantum number but different orbital numbers).

The first stationary value S_1 of the function $S(\omega_{max})$ is a contribution of low-frequency transitions and corresponds to the contribution of intraband transitions. Thus, this value can be used to evaluate the plasma frequency, defined by the intraband transitions in the continuous spectrum, using the formula

$$\omega_p^2 = \frac{N_e e^2}{m\Omega\varepsilon_0} S_1. \qquad (16)$$

The value of ω_p thus obtained can be slightly overestimated due to the contribution of intraband transitions in the discrete spectrum. However, the analysis of the electron density states in shock-compressed xenon plasma has shown that the contribution of such transitions is negligible for the range of densities and temperatures considered.

In addition to the two above-mentioned methods, we evaluate the plasma frequency by considering electrons with energy greater than the Fermi energy E_F as free electrons. Then the concentration n_e of free charge carriers can be calculated by the formula

$$n_e/n = 2\int_{E_F}^{\infty} f(E)g(E)dE, \qquad (17)$$

where $n = N/\Omega$ is the total concentration of ions and atoms and $g(E)$ is the density of electron states. Figure 5 demonstrates an example of the function $g(E)$ for a density of $\rho = 1.1$ g/cm^3.

Figure 6 illustrates the results of calculation of the plasma frequency as a function of the plasma density for all three methods. The values of ω_p obtained in the present study almost coincide with the estimates made in [10, 14] in the low-density region. As ρ increases, a considerable discrepancy between the values of ω_p arises. In this case, the functions of plasma frequency versus density calculated with the use of the Drude formula obtained within the free electron model and by formula (16) nearly coincide, which, to some degree, is a confirmation of the fact that the first stationary value of the function $S(\omega_{max})$ determines the contribution of transitions in the spectrum of free electrons. The values of the plasma frequency calculated by formula (17) also show a rather good agreement with the results of calculation by formula (16).

Knowing the values of the plasma frequency, one can calculate by formula (15) the values of the effective concentration n_e of free charge carriers in plasma. Figure 7 shows n_e as a function of plasma density.

The values of the concentration of free electrons and the corresponding values of the plasma frequency were obtained in [10, 14] within the chemical model of plasma [56]. Here the authors used the Saha equation with regard to the Coulomb attraction in the form of the Debye correction and short-range repulsion in the hard spheres approximation [57, 58]. Thus, the esti-

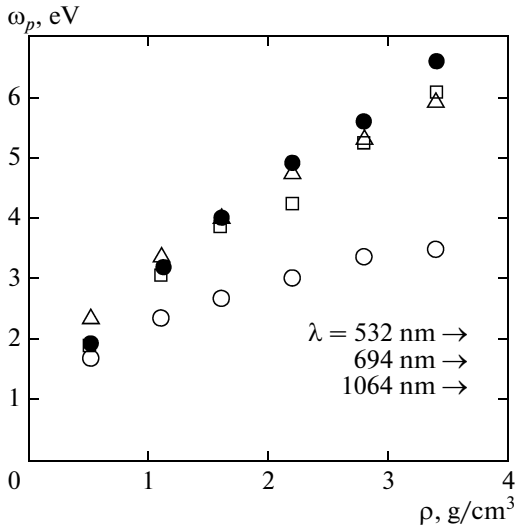

Fig. 6. Plasma frequency as a function of xenon plasma density: plasma density calculated with the use of the Drude formula (12) (closed circles), the results of calculation by formula (16) (squares), estimates of the plasma frequency obtained in [10, 14] (open circles), and plasma frequency calculated with the use of formula (17) for the free charge carrier concentration (triangles). The arrows indicate radiation frequencies corresponding to wavelengths of 1064, 694, and 532 nm.

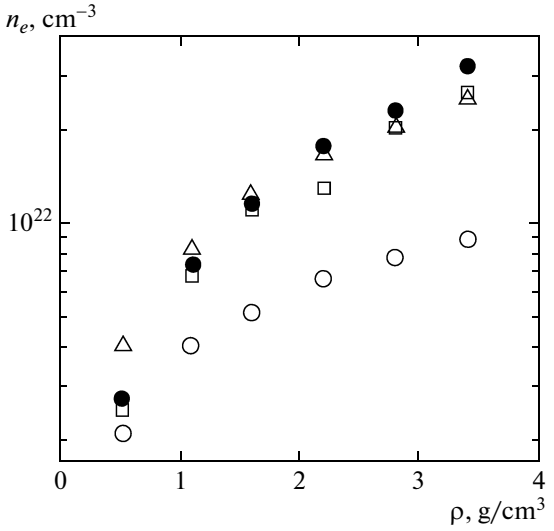

Fig. 7. Electron concentration n_e as a function of plasma density ρ: the values of n_e calculated with the use of formulas (12) and (15) (closed circles), the results of calculation by formulas (16) and (15) (squares), estimates of n_e obtained in [10, 14] (open circles), and the values of n_e calculated with the use of formula (17) (triangles).

mates of n_e and ω_p obtained are related only to the parameters of the plasma created by shock compression of xenon and in no way related to the dependence of the reflectance on density.

In our case, the imaginary part of the DF $\varepsilon^{(2)}$ enters the expressions for both the reflectance and the plasma frequency and uniquely determines their values. Thus, within the approach used in the present study, the calculated values of the plasma frequency are consistent and directly related to the dependence of the reflectance on density. The use of the plasma frequency instead of the concentration of free electrons is consistent with the ideas of [59].

5. REFLECTANCE

5.1. Results

Figure 8 demonstrates the results of calculation of the reflectance as a function of density for different wavelengths of laser radiation and the experimental data from [10–13]. The imaginary part of DF was calculated with the use of formula (8).

For wavelengths of 1064 and 694 nm, the results obtained in the present study are in agreement with experiment both in the absolute value and in the dependence on density in the range of $\rho \geq 1$ g/cm^3. Only a single point lies out in the range of low densities at $\rho = 0.5$ g/cm^3. This discrepancy in the range of low densities may be attributed, in particular, to the fact that, for $\rho = 0.5$ g/cm^3, the ratio of the field penetration depth d to the wavelength λ becomes approximately equal to 0.3 and increases as the density decreases. This fact points to the restricted applicability of the approach in the range of low densities. For higher densities, the parameter $d/\lambda < 0.1$, which guarantees the applicability of this approach in the range of $\rho > 1$ g/cm^3.

For a wavelength of 532 nm and density of $\rho = 1$ g/cm^3, the ratio $d/\lambda = 0.16$; this, in contrast to the case of wavelengths of 1064 and 694 nm, points to the restricted applicability of the long-wavelength approximation at this density. For higher ρ, the ratio $d/\lambda < 0.1$, just as in the case of 1064 and 694 nm. The theoretical values of the reflectance for this wavelength are slightly overestimated compared with the experimental data. However, the relative dependence of the reflectance on density is reproduced.

The arrows in Fig. 8 indicate the values of density ρ at which the frequency of incident radiation coincides with the plasma frequency found in Section 4. Thus, the calculation has shown that there is no cutoff at the plasma frequency; this, to a certain degree, solves the problem posed in the Introduction.

5.2. Errors

We have carried out an analysis for four parameters of calculation: the upper limit of integration in formula (10), the number of particles in a computation cell, the number of **k**-points in the Brillouin zone, and the number of ion configurations.

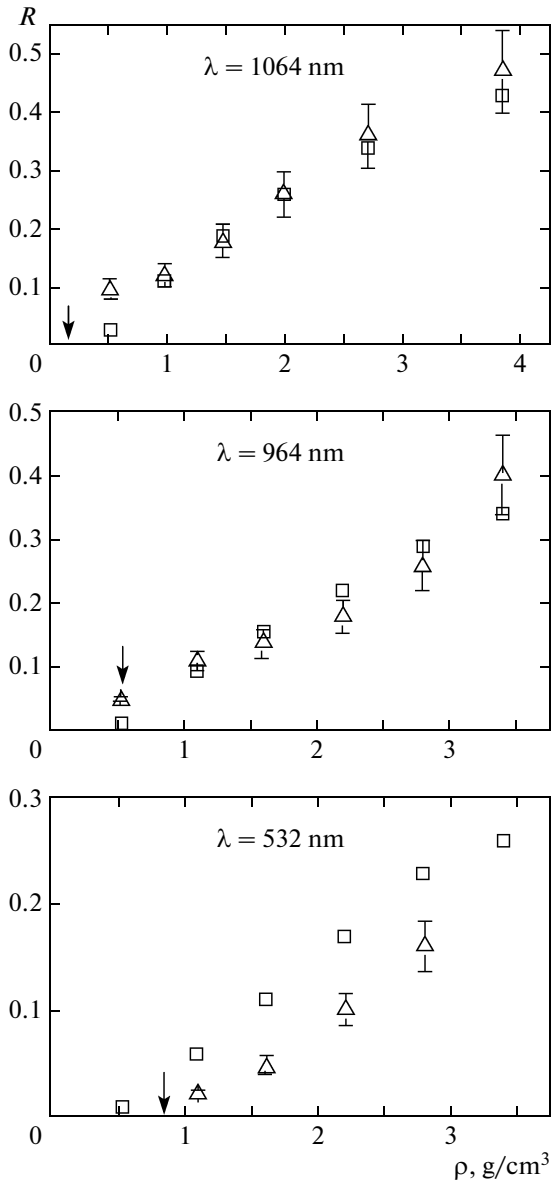

Fig. 8. Reflectance from shock-compressed xenon plasma as a function of density for different wavelengths of incident radiation: experimental data from [10–13] (triangles) and the results of calculation (squares). The arrows indicate the values of density at which the plasma frequency coincides with the frequencies of incident radiation.

The analysis of the dependence of the reflectance on the upper limit of integration in (10) has shown that it suffices to take $\omega_{max} = 40$ eV.

The analysis of the dependence of the results on the number N of particles has shown that, for low density, the results weakly depend on N starting from $N = 16$. An increase in the number of particles leads to a noticeable increase in the computation time. Therefore, especially for low densities, it is important to determine the minimum number of particles in a computation cell for which the results obtained converge. At the same time, as density increases, one should increase the volume of the computation cell. For high densities, the calculations were carried out for 64 particles. To check the convergence with respect to this parameter, we also carried out calculations for 128 particles.

The values of the DF for a given density were averaged over different configurations; this allowed us to determine the relative error of a quantity obtained. As mentioned above, the number of configurations was at least five.

The calculated values of the reflectance shown in Fig. 8 are obtained for one Γ point in the Brillouin zone. To check the convergence of the results with respect to this parameter, we carried out calculations for various numbers of **k** points ranging from 1 to 64. The analysis of the results obtained has shown that an increase in the number of **k** points does not affect the values of the reflectance at given temperatures.

Consider the effect of the computation error of the DF components on the reflectance. The error in the determination of the reflectance is calculated by the standard formula

$$\Delta R = \sqrt{\left(\frac{\partial R}{\partial \varepsilon^{(1)}}\Delta\varepsilon^{(1)}\right)^2 + \left(\frac{\partial R}{\partial \varepsilon^{(2)}}\Delta\varepsilon^{(2)}\right)^2}. \qquad (18)$$

The error $\Delta\varepsilon^{(2)}$ in determining the imaginary part of the DF is the root-mean-square deviation of $\varepsilon^{(2)}$ when averaging over different configurations. As the number of configurations increases, the values of $\Delta\varepsilon^{(2)}$ decrease. The errors in determining the imaginary $\Delta\varepsilon^{(2)}$ and real $\Delta\varepsilon^{(1)}$ parts of the DF are related by the formula

$$\Delta\varepsilon^{(1)}(\omega) = \frac{2}{\pi}\int_0^\infty \frac{\Delta\varepsilon^{(2)}(\omega')\omega'}{\omega'^2 - \omega^2}d\omega' = \frac{2}{\pi}\int_0^\infty \frac{\gamma\varepsilon^{(2)}(\omega')\omega'}{\omega'^2 - \omega^2}d\omega', \qquad (19)$$

where γ is the relative error in determining the imaginary part of the DF, which is assumed to be independent of frequency.

In the range of low densities, the relative error in determining the imaginary part of the DF is maximal and does not exceed 15%. For the minimum value of ρ, the relative error $\Delta\varepsilon^{(1)}/\varepsilon^{(1)}$ is about 1.5%; in this case, the ratio of derivatives is $(\partial R/\partial\varepsilon^{(1)})/(\partial R/\partial\varepsilon^{(2)}) \ll 1$. Thus, for low density, the imaginary part of the DF makes a key contribution to the error in determining the reflectance, which in this case amounts to about 30%.

As density increases to $\rho = 3.84$ g/cm^3, the derivatives of the reflectance with respect to the DF components, as well as the relative errors $\varepsilon^{(1)}$ and $\varepsilon^{(2)}$, become equal to each other. Thus, the imaginary and real parts of the DF make equal contributions to ΔR. The abso-

lute value of ΔR increases, while the relative error noticeably decreases to a value of less than 5%. Therefore, for large values of density, there is no need to increase the accuracy of determination of the imaginary part of DF.

6. DISCUSSION OF THE RESULTS

Figure 9 demonstrates the reflectance of laser radiation with wavelength 1064 nm as a function of density. The solid curve corresponds to the case of collisionless plasma when a cutoff on the plasma frequency should be observed; the triangles represent experimental data of [10], and the dashed curve represents an approximation to the experimental data of [10] with the collision frequency in the Born approximation [14]. These curves and symbols are analogous to those shown in Fig. 1. The experimental data show that there is no cutoff at the plasma frequency. The Drude formula with nonzero collision frequency also provides no explanation to the experimental data.

In [14–16], the authors assumed that, during shock-wave compression of xenon, the density does not increase stepwise, but there exists a region of finite width in which density smoothly increases to a prescribed value. Thus, the wave front has a finite width, and laser radiation is reflected not only from xenon plasma, but also from the wave front. The width of the front is about 1 μm, which is comparable with the wavelength of the incident radiation. This assumption appreciably improves the agreement with experiment compared with the assumption of an abrupt front. Figure 9 shows that the results of approximation of experimental data within a model with such a wide front allow one to accurately describe the dependence of the reflectance on density at a wavelength of 1064 nm (however, at other wavelengths, the accuracy is lower). As mentioned above, the assumption of the broadening of the front has no independent experimental confirmation.

The diamonds connected by a dot-and-dash curve correspond to the results of calculation in [29]. One can see that the results of [29] appreciably better agree with experiment compared to the case when the Drude formula is used. However, there is also an appreciable discrepancy with experiment in the range of low densities. To improve the agreement with the experimental results of [10], Desjarlais [29] additionally assumed that the energy gap between free and bound states increases. He draws an analogy with the spectrum of semiconductors, where the underestimation of the energy band gap was observed when calculating the electron state density within DFT. As shown in [39], these corrections appear in the expression for the imaginary part of the DF as follows:

$$\varepsilon^{(2)}_{\text{gap}}(\omega) = \left[\frac{\hbar\omega}{\hbar\omega - \Delta}\right]^2 \varepsilon^{(2)}(\omega), \qquad (20)$$

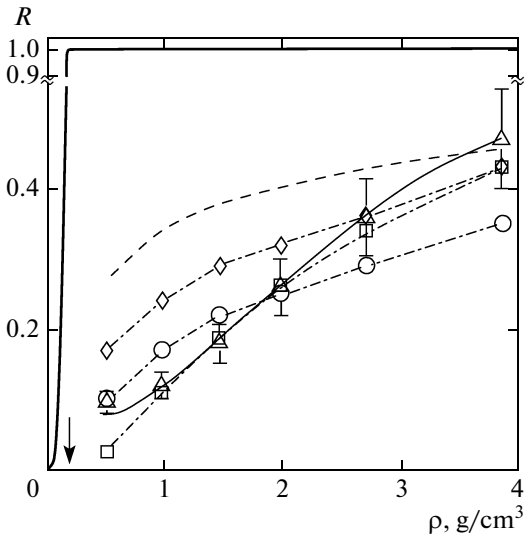

Fig. 9. Reflectance as a function of density for a wavelength of 1064 nm: the case of collisionless plasma when a cutoff is observed at the plasma frequency (solid heavy curve), approximation of experimental results with the use of the Drude model with the collision frequency in the Born approximation [14] (dashed curve), the Drude model with regard to the front width [14–16] (thin curve), experimental data from [10] (triangles), the results of [29] (diamonds), the results of [29] obtained with the use of corrections to the energy gap width between free and bound states (circles), and results of the present study (squares). The arrow indicates the value of plasma density at which the frequency of incident radiation coincides with the plasma frequency.

where Δ is a correction that increases the gap between bound and free states. In [29], Desjarlais proposed to artificially increase the gap by $\Delta = 2.5$ eV. In this case, using expression (20), one can approximately take into account the contributions to the DF and the reflectance that are not taken into account within the random phase approximation.

The results of calculation of the reflectance with regard to this correction are shown in Fig. 9 by circles connected by a dot-and-dash curve. This slightly improves the agreement between the results of calculation [29] and experimental results at low densities. In this case, the values of the reflectance at high densities are underestimated. The functions of the reflectance versus density [29] with and without regard to the correction are almost parallel. Thus, the introduction of the correction affects only the absolute values and does not change the dependence of the reflectance on density.

Above, in Fig. 5, we demonstrated the density of electron states for a xenon plasma density of $\rho = 1.1$ g/cm^3 calculated within the DFT approach. One can see that an energy gap arises between free states ($E - E_F > 0$) and a discrete level of $E \approx -10$ eV.

In the general case, as shown in [52], the representation of an electron spectrum in dense plasma as a

combination of a continuous spectrum of free states and a discrete spectrum of bound electrons separated by an energy gap is not correct. Thus, the validity of the corrections introduced in [29] for calculating the properties of warm dense matter requires further analysis and refinement.

The results of [29] were obtained under the assumption of an abrupt shock-wave front and agree well enough with experiment. Thus, in spite of the fact that, in the general case, the front is not ideal and has nonzero width, the effect of the front broadening on the reflectivity of shock-compressed xenon is obviously overestimated in [14–16], because the results of the first-principles calculations agree with experimental data to the same degree of accuracy without invoking the front broadening conjecture.

The results of calculations obtained in the present study noticeably better (compared with [29]) agree with experiment both in absolute value and in the dependence on density without introducing corrections to the energy gap width. The slope of the dependence of the reflectance on density obtained in the present study is appreciably greater than that given in [29]. The absolute values given in [29] are much greater than the results calculated in the present study in the range of $\rho < 3$ g/cm^3 (by a factor of eight for the minimum value of density) and are twice the measured values in [10]. As mentioned above, the main difference between the approach used in the present study and the approach of [29] is the use of expression (8) for the longitudinal component of the tensor instead of the transverse expression (5), which gives a more correct result compared with the Kubo–Greenwood formula within DFT.

In the present study, we did not consider the effect of the actual width of the wave front in xenon. However, we cannot rule out the fact that, for the boundary domains of the range of parameters considered, this factor may contribute to the reflectivity of shock-compressed xenon plasma, although to an appreciably smaller degree than that supposed in [14–16].

7. CONCLUSIONS

Within density functional theory, we have calculated the reflectance from shock-compressed xenon plasma as a function of density for different values of wavelength. On the basis of the results obtained, we can draw two basic conclusions.

1. The application of the expression for the longitudinal dielectric tensor gives much better agreement with experiment compared with both the Drude model with the collision frequency in the Born approximation and the DFT approach with the use of a formula for the transverse component of the dielectric tensor (the Kubo–Greenwood formula). We have considered the long-wavelength limits.

2. We have proposed a method for calculating the plasma frequency within DFT that is based on the rule of sums. This approach allows one to derive the plasma frequency, as well as the reflectance and the conductivity, from the same expression for the dielectric tensor. Thus, the density dependences obtained for these parameters turn out to be self-consistent and internally correlated with each other.

ACKNOWLEDGMENTS

We are grateful to V.B. Mintsev and Yu.B. Zaporozhets for providing a constant supply of information on the results of measurements, as well as to M. Desjarlais for useful discussions and remarks. The computations were carried out on the K-100 cluster at the Keldysh Institute of Applied Mathematics, Russian Academy of Sciences, and on the cluster of the Joint Supercomputer Center, Russian Academy of Sciences.

This work was supported in part by the Presidium of the Russian Academy of Sciences within the Fundamental Research program No. 43 "Fundamental Problems of Mathematical Modeling" and by the Russian Foundation for Basic Research (project nos. 14-08-31694-mol_a (I.M.S.) and 13-01-12070-ofi-m). The work of V.V.S. was supported by the National Research University Higher School of Economics within the Fundamental Research Program.

REFERENCES

1. G. W. Collins, P. M. Celliers, D. M. Gold, L. B. Da Silva, and R. Cauble, Contrib. Plasma Phys. **39**, 13 (1999).
2. P. M. Celliers, G. W. Collins, L. B. Da Silva, D. M. Gold, R. Cauble, R. J. Wallace, M. E. Foord, and B. A. Hammel, Phys. Rev. Lett. **84**, 5564 (2000).
3. P. Loubeyre, P. M. Celliers, D. G. Hicks, E. Henry, A. Dewaele, J. Pasley, J. Eggert, M. Koenig, F. Occelli, K. M. Lee, R. Jeanloz, D. Neely, A. Benuzzi-Mounaix, D. Bradley, M. Bastea, S. Moon, and G. W. Collins, High Pressure Res. **24**, 25 (2004).
4. P. M. Kowalski, S. Mazevet, D. Saumon, and M. Challacombe, Phys. Rev. B: Condens. Matter **76**, 075112 (2007).
5. P. M. Celliers, P. Loubeyre, J. H. Eggert, S. Brygoo, R. S. McWilliams, D. G. Hicks, T. R. Boehly, R. Jeanloz, and G. W. Collins, Phys. Rev. Lett. **104**, 184503 (2010).
6. F. Soubiran, S. Mazevet, C. Winisdoerffer, and G. Chabrier, Phys. Rev. B: Condens. Matter **86**, 115102 (2012).
7. G. Huser, N. Ozaki, and T. Sano, Phys. Plasmas **20**, 122703 (2013).
8. M. A. Morales, J. M. McMahon, C. Pierleoni, and D. M. Ceperley, Phys. Rev. Lett. **110**, 065702 (2013).
9. F. Soubiran, S. Mazevet, C. Winisdoerffer, and G. Chabrier, Phys. Rev. B: Condens. Matter **87**, 165114 (2013).
10. V. B. Mintsev and I. B. Zaporozhets, Contrib. Plasma Phys. **29**, 493 (1989).

11. Yu. B. Zaporozhets, V. B. Mintsev, V. K. Gryaznov, and V. E. Fortov, in *Physics of Extreme States of Matter—2002*, Ed. by V. E. Fortov et al. (Institute of Problems of Chemical Physics of the Russian Academy of Sciences, Chernogolovka, 2002), p. 188 [in Russian].
12. Yu. B. Zaporozhets, V. B. Mintsev, V. K. Gryaznov, V. E. Fortov, H. Reinholz, and G. Röpke, in *Physics of Extreme States of Matter—2004*, Ed. by V. E. Fortov et al. (Institute of Problems of Chemical Physics of the Russian Academy of Sciences, Chernogolovka, 2004), p. 140 [in Russian].
13. Y. Zaporozhets, V. Mintsev, V. Gryaznov, V. E. Fortov, H. Reinholz, T. Raitza, and G. Röpke, J. Phys. A: Math. Gen. **39**, 4329 (2006).
14. H. Reinholz, G. Röpke, A. Wierling, V. Mintsev, and V. Gryaznov, Contrib. Plasma Phys. **43**, 3 (2003).
15. H. Reinholz, G. Röpke, I. Morozov, V. Mintsev, Yu. Zaporogets, V. Fortov, and A. Wierling, J. Phys. A: Math. Gen. **36**, 5991 (2003).
16. H. Reinholz, Y. Zaporoghets, V. Mintsev, V. Fortov, I. Morozov, and G. Röpke, Phys. Rev. E: Stat., Nonlinear, Soft Matter Phys. **68**, 036403 (2003).
17. Yu. V. Petrov and N. A. Inogamov, JETP Lett. **98** (5), 278 (2012).
18. G. E. Norman, S. V. Starikov, and V. V. Stegailov, J. Exp. Theor. Phys. **114** (5), 792 (2012).
19. N. A. Medvedev, A. E. Volkov, K. Schwartz, and C. Trautmann, Phys. Rev. B: Condens. Matter **87**, 104103 (2013).
20. B. Rethfeld, A. Rämer, N. Brouwer, N. Medvedev, and O. Osmani, Nucl. Instrum. Methods Phys. Res., Sect. B **327**, 78 (2014).
21. F. C. Kabeer, E. S. Zijlstra, and M. E. Garcia, Phys. Rev. B: Condens. Matter **89**, 100301 (2014).
22. W. Kohn and L. J. Sham, Phys. Rev. Sect. A **140**, A1133 (1965).
23. W. Kohn, *Nobel Lecture on Physics* (The Nobel Foundation, Stockholm, 1999).
24. P. A. Zhilyaev and V. V. Stegailov, Vychisl. Metody Program. **13**, 37 (2012).
25. N. A. Skorikov, M. A. Korotin, E. Z. Kurmaev, and S. O. Cholakh, J. Exp. Theor. Phys. **115** (6), 1048 (2012).
26. M. G. Kostenko, A. A. Rempel', and A. V. Lukoyanov, J. Exp. Theor. Phys. **116** (6), 945 (2013).
27. T. V. Perevalov and A. V. Shaposhnikov, J. Exp. Theor. Phys. **116** (6), 995 (2013).
28. I. P. Rusinov, I. A. Nechaev, and E. V. Chulkov, J. Exp. Theor. Phys. **116** (6), 1006 (2013).
29. M. P. Desjarlais, Contrib. Plasma Phys. **45**, 300 (2005).
30. M. Gajdoš, K. Hummer, G. Kresse, J. Furthmüller, and F. Bechstedt, Phys. Rev. B: Condens. Matter **73**, 045112 (2006).
31. M. French and R. Redmer, Phys. Plasmas **18**, 043301 (2011).
32. M. E. Povarnitsyn, D. V. Knyazev, and P. R. Levashov, Contrib. Plasma Phys. **52**, 145 (2012).
33. Y. Ping, D. Rocca, and G. Galli, Phys. Rev. B: Condens. Matter **87**, 165203 (2013).
34. P. A. Zhilyaev, G. E. Norman, I. M. Saitov, and V. V. Stegailov, Dokl. Phys. **58** (7), 277 (2013).
35. N. D. Mermin, Phys. Rev. Sect. A **137**, A1441 (1965).
36. R. Kubo, J. Phys. Soc. Jpn. **12**, 570 (1957).
37. D. A. Greenwood, Proc. Phys. Soc. **71**, 585 (1958).
38. T. R. Mattsson and R. J. Magyar, AIP Conf. Proc. **1195**, 797 (2009).
39. R. Del Sole and R. Girlanda, Phys. Rev. B: Condens. Matter **48**, 11789 (1993).
40. A. Starace, Phys. Rev. A: At., Mol., Opt. Phys. **3**, 1242 (1971).
41. D. A. Frank-Kamenetskii, *Lectures on Plasma Physics* (Atomizdat, Moscow, 1968) [in Russian].
42. H. Ehrenreich and M. H. Cohen, Phys. Rev. **115**, 786 (1959).
43. S. L. Adler, Phys. Rev. **126**, 413 (1962).
44. N. Wiser, Phys. Rev. **129**, 62 (1963).
45. G. Kresse and J. Hafner, Phys. Rev. B: Condens. Matter **47**, 558 (1993).
46. G. Kresse and J. Hafner, Phys. Rev. B: Condens. Matter **49**, 14251 (1994).
47. G. Kresse and J. Furthmüller, Phys. Rev. B: Condens. Matter **54**, 11169 (1996).
48. J. P. Perdew, A. Ruzsinszky, G. I. Csonka, O. A. Vydrov, G. E. Scuseria, L. A. Constantin, X. Zhou, and K. Burke, Phys. Rev. Lett. **100**, 136406 (2008).
49. S. Nosé, J. Chem. Phys. **81**, 511 (1984).
50. W. G. Hoover, Phys. Rev. A: At., Mol., Opt. Phys. **31**, 1695 (1985).
51. J. P. Perdew, K. Burke, and M. Ernzerhof, Phys. Rev. Lett. **77**, 3865 (1996).
52. A. V. Lankin and G. E. Norman, J. Phys. A: Math. Gen. **42**, 214032 (2009).
53. P. Drude, Ann. Phys. **306**, 566 (1900).
54. P. Drude, Ann. Phys. **308**, 369 (1900).
55. L. D. Landau and E. M. Lifshitz, *Course of Theoretical Physics*, Volume 8: *Electrodynamics of Continuous Media* (Fizmatlit, Moscow, 2005; Butterworth–Heinemann, Oxford, 2005).
56. W. Ebeling, Physica (Amstardam) **43**, 293 (1969).
57. V. Fortov, V. Gryaznov, V. Mintsev, V. Ya. Ternovoi, I. L. Iosilevski, M. V. Zhernokletov, and M. A. Mochalov, Contrib. Plasma Phys. **41**, 215 (2001).
58. V. E. Fortov, V. Ternovoi, M. V. Zhernokletov, M. A. Mochalov, A. L. Mikhailov, A. S. Filimonov, A. A. Pyalling, V. B. Mintsev, V. K. Gryaznov, and I. L. Iosilevski, J. Exp. Theor. Phys. **97** (2), 259 (2003).
59. M. S. Murillo, J. Weisheit, S. B. Hansen, and M. W. C. Dharma-wardana, Phys. Rev. E: Stat., Nonlinear, Soft Matter Phys. **87**, 063113 (2013).

Translated by I. Nikitin